THE JOURNAL OF PHYSICAL CHEMISTRY A

pubs.acs.org/JPCA Article

Ultrafast Proton Transfer Dynamics on the Repulsive Potential of the Ethanol Dication: Roaming-Mediated Isomerization versus Coulomb Explosion

Enliang Wang, Xu Shan, Lei Chen, Thomas Pfeifer, Xiangjun Chen, Xueguang Ren,* and Alexander Dorn*

Cite This: J. Phys. Chem. A 2020, 124, 2785−2791

Read Online

ACCESS | Metrics & More | Article Recommendations | Supporting Information

ABSTRACT: If a molecular dication is produced on a repulsive potential energy surface (PES), it normally dissociates. Before that, however, ultrafast nuclear dynamics can change the PES and significantly influence the fragmentation pathway. Here, we investigate the electron-impact-induced double ionization and subsequent fragmentation processes of the ethanol molecule using multiparticle coincident momentum spectroscopy and ab initio dynamical simulations. For the electronic ground state of the ethanol dication, we observe several fragmentation channels that cannot be reached by direct Coulomb explosion (CE) but require preceding isomerization. Our simulations show that ultrafast hydrogen or proton transfer (PT) can stabilize the repulsive PES of the dication before the direct CE and form intermediate H_2 or H_2O. These neutrals stay in the vicinity of the precursor, and roaming mechanisms lead to isomerization and finally PT resulting in emission of H_3^+ or H_3O^+. The present findings can help to understand the complex fragmentation dynamics of molecular cations.

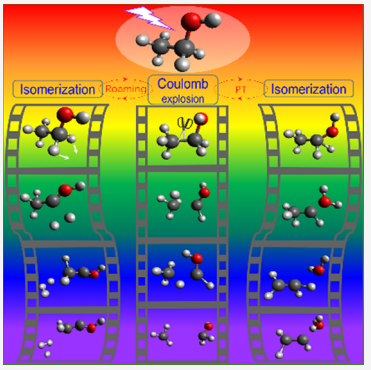

INTRODUCTION

The removal of two electrons from a neutral molecule is a process of fundamental interest in chemical physics. An understanding of the structure of molecular dications and the dynamics of dissociation processes is relevant to understand and model the behavior of gaseous plasmas as well as the ionosphere and astrophysical environment.[1,2] Significant rearrangement of the chemical bonds can be initiated due to the considerable internal energy in the dications, leading to various Coulomb explosion (CE) channels.[3,4]

Of particular interest in the present work are the very fast hydrogen and proton transfer mechanisms (for general discussion, we use PT to represent both hydrogen and proton transfer) that are relevant in various fields of physics, chemistry, and biology.[5−7] In particular, PT is a common and fundamental process in organic chemistry and molecular biology as all organic compounds contain a large fraction of hydrogen atoms.[8] PT can form different isomers and therefore change functional properties of the molecule. In particular, proton-translocating tautomerization of DNA base pairs has been suggested as a cause of mutations, which have been broadly studied in the past 50 years.[9−13]

PT-initiated isomerization of a molecule affects chemical reactions in solution. A changing chemical environment of a biomolecule can induce conformational or isometric transformations.[3] Recently, it was found for amino acids that the intramolecular PT from the carboxyl (−COOH) group to the amino ($-NH_2$) group will reduce the molecule's total energy in aqueous solution or in crystals and form a so-called "zwitterion".[14] As being the lightest element, hydrogen exhibits ultrafast dynamics whether in classical migration[15,16] or being subject to nuclear quantum effects.[11,17−20] For example, in ionized glycine, the timescale of PT was determined to be less than 50 fs.[16] In a recent work, Richter et al. showed that intermolecular PT is fast enough to influence the electronic decay due to the coupling of the electron and nuclear dynamics in water clusters.[21] Even on the repulsive PES of the dication where the system is expected to rapidly dissociate, PT can stabilize the dication. For example, Maclot et al. showed for double ionization of glycine that CE competes with ultrafast intramolecular PT evolving within ∼30 fs resulting in stable glycine dication.[15]

On the other hand, PT can lead to isomerization during molecular fragmentation.[22,23] As a prototype, the PT in acetylene has been studied by pump-probe experiments,[24] X-ray core−shell ionization,[25] and α-particle irradiation.[26] Furthermore, if a process involves multiple PT,[9,27] more complex fragments can be formed like H_3^+ emitted from organic molecules.[28−32] In this respect, Ekanayake et al.

Received: March 9, 2020
Published: March 11, 2020

https://dx.doi.org/10.1021/acs.jpca.0c02074
J. Phys. Chem. A 2020, 124, 2785−2791

performed time-resolved pump-probe experiments using femtosecond laser pulses and ab initio molecular dynamics (AIMD) simulations. For different alcohols, they found that, for H_3^+ production, the intermediate roaming of H_2 plays an important role and that the timescale for the fragmentation process is between 100 and 260 fs.[30,32] The calculation of the respective reaction pathways is challenging for conventional transition-state (TS) theory since H_2 roaming may explore large regions of the PES and bypass saddle points entirely.[33]

In the present work, we carry out combined experimental and theoretical studies concerning the PT-induced isomerization and CE of the ground-state ethanol dication. Fragment ion and electron momentum spectroscopies, accompanied by molecular dynamics calculations, allow us to directly identify the different fragmentation channels and understand the underlying mechanisms and the role of PT. It is found that, while double ionization leads to a repulsive PES, fast PT can stabilize the dication before CE and then open several isomerization channels. Here, we focus on three channels, including one CE channel and two isomerization channels, for emission of H_3^+ and H_3O^+:

$$CH_3CH_2OH^{2+} \rightarrow CH_3^+ + CH_2OH^+ \quad (1)$$

$$CH_3CH_2OH^{2+} \rightarrow H_3^+ + C_2H_3O^+ \quad (2)$$

$$CH_3CH_2OH^{2+} \rightarrow H_3O^+ + C_2H_3^+ \quad (3)$$

The theoretical analysis of the molecular dynamics using the AIMD simulation and the static energy calculation of PESs and TSs shows that all three channels are open on the ground-electronic-state PES of $CH_3CH_2OH^{2+}$. As the ethanol dication reached in a vertical transition is in a repulsive state along the C_α–C_β bond cleavage (carbon connecting to the hydroxyl is defined as C_α, while the terminal one is C_β), it is expected to dissociate via CE. In the same electronic state, however, new fragmentation channels are opened if a stabilization process can take place before CE. There are three possible ways to stabilize the ethanol dication, i.e., PT from C_α to C_β ($CH_3CH_2OH^{2+} \rightarrow CH_4CHOH^{2+}$), from C_α to hydroxyl ($CH_3CH_2OH^{2+} \rightarrow CH_3CHOH_2^{2+}$ forming an intermediate H_2O group), and forming an intermediate H_2 group. The Mulliken charge analysis shows that the intermediates like H_2 and H_2O are neutral groups. Their long-time motion around the parent molecule can be regarded as a roaming chemical process.[33,34] We demonstrate that the intramolecular PT and roaming dynamics play key roles in stabilizing the ethanol dication and altering significantly the fragmentation pathways.

RESULTS

The experiments were performed by electron-impact ionization of ethanol using two different spectrometers at similar impact-energies of 91 and 100 eV (see Supporting Information for details). The dissociative CE channels were identified by analyzing the ion-ion time correlation map of both ions detected on a time- and position-sensitive detector. In the diagram shown in Figure 1a, the time of flight (TOF) of the ion detected second is plotted against the ion detected first. Sharp coincidence lines with a slope of −1 are observed for channels 1–3 (purple-shaded labels) confirming that these are pure two-body dissociation processes. For all other channels labeled in Figure 1a, the ethanol dications dissociate into three or more fragments including two ions and neutrals. The most intense region in the center of Figure 1a originates from

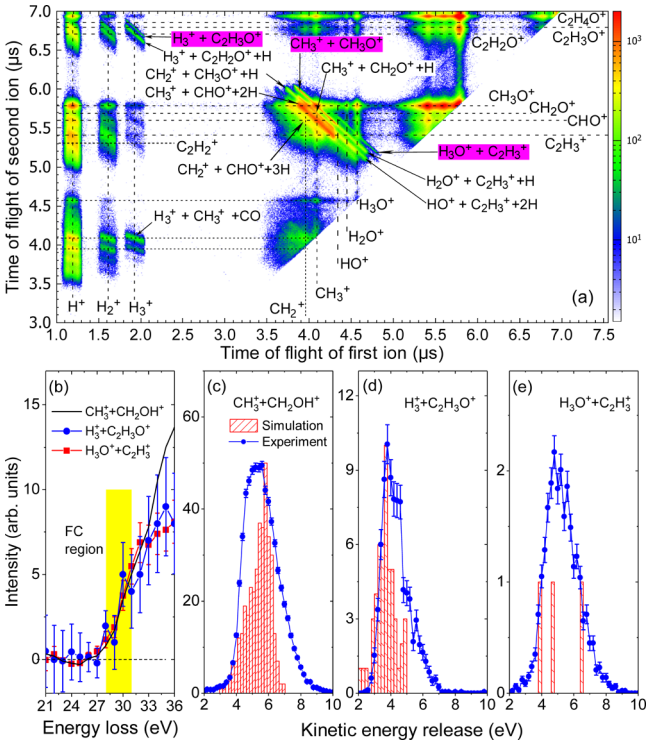

Figure 1. (a) Time correlation map of two measured ions obtained by plotting the time of flight of the second-hit ion against the first hit on the detector. Electron-impact energy is 100 eV. The labels for two-body dissociation channels are shaded. (b) Projectile energy loss spectra for the three studied channels measured using a reaction microscope at an impact energy of 91 eV. The FC region in this figure means the Franck–Condon region. (c–e) Experimental and simulated kinetic energy release (KER) distributions for the three studied channels. The experimental KERs are obtained from the data in panel (a).

reactions similar to channel 1 but with hydrogen loss for one or both fragment ions. In addition, there are coincidences for $C_2H_3^+ + H_{3-n}O^+ + nH$ (n = 1, 2), again with one or two neutral hydrogens emitted. Finally, there are three-body channels including a H_n^+ ion with n = 1–3 in the time-of-flight interval of the first detected ion between 1 and 2.2 μs. The corresponding coincidence lines are broad and strongly overlapping along the y axis since the undetected neutral fragment is rather heavy and carries considerable momentum. In an earlier ion-ion coincidence measurement for ethanol using intense infrared laser pulses for ionization, more pure two-body fragmentation channels without neutral hydrogen loss were found than in the present measurement.[35] The reason most likely is that strong field double ionization evolves as sequential single ionization from the outermost valence electrons. For the present particle-impact ionization, both electrons are removed simultaneously and not necessarily from the outermost shell such that more internal energy is present in the dication that can lead to the emission of neutrals. In the following, we will concentrate our discussion to the two-body channels 1–3.

In one of our measurements, one of the final state electrons was detected in coincidence with the two ions. Thus, the projectile energy loss spectra for the different fragmentation channels were obtained (Figure 1b). The spectra show onsets at about 28 eV for all three channels, meaning that these are initiated by the removal of two electrons from the outermost

https://dx.doi.org/10.1021/acs.jpca.0c02074
J. Phys. Chem. A 2020, 124, 2785–2791

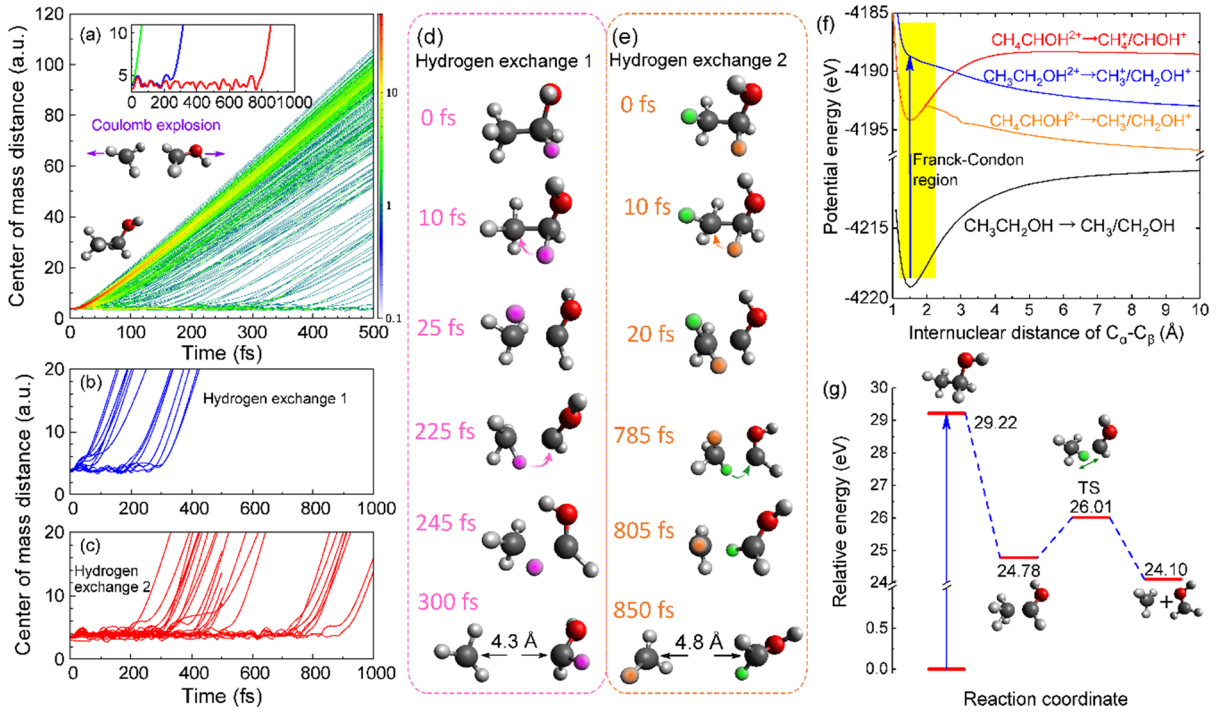

Figure 2. Fragmentation dynamics of the Coulomb explosion channels. Center-of-mass distance as a function of simulation time (a) for all trajectories, (b) for the one hydrogen exchange mechanism, and (c) for the two hydrogen exchange mechanism. The intermediate dicationic structures for two typical trajectories for (d) one hydrogen exchange and (e) two hydrogen exchange. (f) Potential energy curves as a function of C_α−C_β bond length. (g) The energy as a function of the reaction coordinate for the transition state corresponding to hydrogen transfer. The fragmentation paths in panels (d) and (e) correspond to the blue and red curves in the insets of panel (a), respectively.

orbital of the ethanol reaching the dicationic ground state.[36] The range marked in yellow indicates the energy region for a vertical ionization from the neutral ground state to the dicationic ground state of ethanol. The AIMD simulations (see Supporting Information for details) show that the two-body CE process is dominated by channel 1 that contributes about 18.2% to the total simulated trajectories. For channel 2, the branching ratio is 2.6%, and only three out of 2000 trajectories ended up in channel 3. For all of the calculations, the charge states of final fragments are obtained from the Mulliken population analysis, which confirms that the studied channels produce two cations. The simulated and experimental kinetic energy release (KER) distributions presented in Figure 1c−e show good agreement within the limited statistical significance of the trajectory number.

The fragmentation dynamics of the CE channel 1 is shown in Figure 2. Panel (a) presents the center-of-mass (COM) distance between CH_3^+ and CH_2OH^+ as a function of time. This diagram shows two main features: (i) most of the molecules start to dissociate directly within 50 fs, giving rise to the red region formed by a large number of trajectories; (ii) a small fraction shows dissociation after some time delay ranging from several tens of femtoseconds to more than 500 fs. During this time, there is vibration between the two subunits manifesting in the oscillations of the blue and red curves in the inset of Figure 2a. To form the long-lived dications, a fast (less than 50 fs) stabilization mechanism is required, which is exactly the ultrafast hydrogen migration. The insets in panel (a) show three typical trajectories corresponding to three mechanisms indicated by green, blue, and red curves: (i) fast CE (FCE) where the two charged fragments dissociate directly once a dication is formed; (ii) delayed CE with one hydrogen exchange (DCE-HE1); and (iii) delayed CE with two hydrogen exchange (DCE-HE2). For DCE-HE1, one hydrogen transfers from C_α to C_β in the first step, and subsequently, the identical one transfers back to C_α before C_α−C_β breakage. For DCE-HE2, however, another hydrogen belonging to C_β in the neutral ethanol transfers back to C_α in the second step.

The detailed analysis of the simulated fragmentation dynamics shows that dissociation through the DCE-HE1 mechanism is statistically faster than DCE-HE2 as depicted by their COM distances as a function of time in Figure 2b,c, respectively. For DCE-HE1, the C_α−C_β bond starts to dissociate before about 300 fs. For DCE-HE2, however, the lifetime is longer than 300 fs for most of the cases. The intermediate steps of the two fragmentation pathways are shown in Figure 2d,e. For both mechanisms, the ultrafast hydrogen exchange is completed within about 20 fs. The lifetime difference of DCE-HE1 and DCE-HE2 is due to the different orientations of the transferred or exchanged hydrogen (defined as H_1 shown by the pink ball in Figure 2d or H_2 by the green one in Figure 2e) relative to the C_α−C_β bond. For DCE-HE1, the angle $\angle H_1C_\beta C_\alpha$ is always a pointed angle (<90°). Thus, H_1 is always very close to C_α making the back transfer easy to occur. For DCE-HE2, the angle $\angle H_2C_\beta C_\alpha$ is an obtuse angle at the very beginning. The hydrogen exchange can occur only after a rotation of the CH_4 group relative to the C_α−C_β bond until reaching a small enough distance between H_2 and C_α. Figure 2f shows the PESs (see Supporting Information for details) as a function of the C_α−C_β bond length. The blue arrow in the Franck−Condon region indicates the most probable vertical ionization from neutral to the dicationic ground state. Due to the repulsive PES, the dication can dissociate through FCE in principle. On the ground-state

https://dx.doi.org/10.1021/acs.jpca.0c02074
J. Phys. Chem. A 2020, 124, 2785−2791

PES of the ethanol dication, however, there are local minimum energy points corresponding to equilibrium geometries. As shown by the red curve in Figure 2f, a bound state is formed if one hydrogen transfers from C_α to C_β. The resulting red curve presents a potential energy barrier that is even higher than the most probable vertical transition point. As a result, CH_4CHOH^{2+} does not dissociate via C_α–C_β bond breakage both in experiments and in the simulation. The crossing between the two PESs of $CH_3CH_2OH^{2+}$ and CH_4CHOH^{2+} forms a TS connecting these two isomers. As the rigid PES scanning freezes all degrees of freedom, such PES may be different from the actual situation of the fragmentation. As shown by the orange curve in Figure 2f, the relaxed PES scanning indicates that there will be isomeric transformation from CH_4CHOH^{2+} to $CH_3CH_2OH^{2+}$ with increasing C_α–C_β length. The corresponding TS and the pathway are confirmed by the intrinsic reaction coordinate (IRC) calculation as shown in Figure 2g.

For channel 2 with the H_3^+ and $C_2H_3O^+$ fragments, Figure 3 shows the COM distance between these two groups as a function of time. H_3^+ emission appears from ∼100 to ∼500 fs, which is in agreement with the previous time-resolved pump-probe studies.[30,32] The trajectory analysis shows that there are five possible ways of forming H_3^+, which all include the formation and subsequent roaming of one intermediate H_2 as shown in Figure 4: C_α emits one H_2 molecule, which captures one proton (a) from C_β or (b) from the hydroxyl group ((c) C_β as hydrogen and proton donors, (d) C_β and hydroxyl as hydrogen and proton donors, and (e) C_α, C_β, and hydroxyl as hydrogen and proton donors forming H_3^+). For all of the cases, ultrafast PT and H_2 formation can occur within about 25 fs, which stabilizes the ethanol dication concerning the C_α–C_β bond breakage. For the reaction channels shown in Figure 4c–e, the dynamics starts by hydrogen transfer from C_α to C_β and is followed by emission of H_2 from the CH_4 group. Thus, there are generally two ways to produce the intermediate roaming H_2: (i) the direct formation from C_α as shown in Figure 4a,b and (ii) the indirect way from C_β as shown in Figure 4c–e.

For the first mechanism, roaming H_2 is formed within about 20 fs, and finally, one proton can be captured from the neighboring carbon or hydroxyl before 200 fs. For the second mechanism, however, no proton capture from neighboring carbon is observed. The proton can be captured from the parent carbon (C_β) or from hydroxyl for which rather long-time roaming (longer than 200 fs) is needed. The TS analysis and IRC path calculations confirm the above-simulated pathways. Figure 4f,g shows the pathways corresponding to H_2 formation from C_α and C_β, respectively. For the first case, the intermediate H_2 can directly attract one proton from C_β via TSa-1 → TSa-2 or from hydroxyl via TSb. For the second case, however, proton capture can happen only after PT from C_α to C_β as shown by TS-2 in Figure 4g, which is in line with the MD simulations.

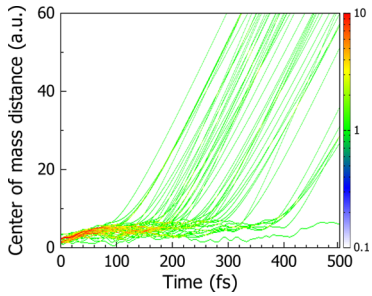

Figure 3. Center-of-mass distance between H_3^+ and $C_2H_3O^+$ as a function of simulation time for H_3^+ formation channel.

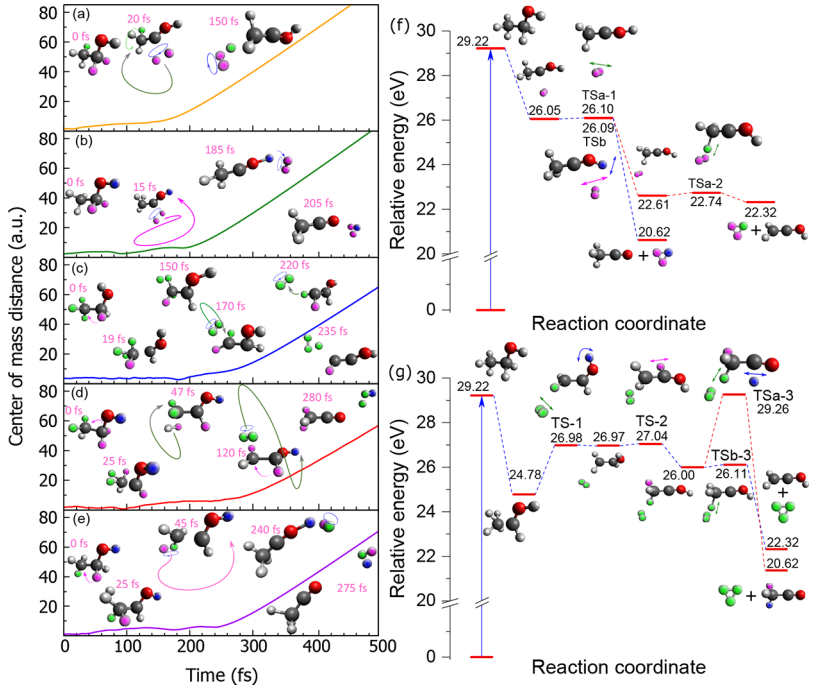

Figure 4. Pathways for H_3^+ formation dynamics. Panels (a–e) show five typical trajectories in which the short curved arrows show hydrogen transfer patterns, the long curved arrows show the roaming path of H_2, and the circles with arrow show rotation of H_2. Panels (f) and (g) show transition states and reaction paths corresponding to H_2 formation from C_α and C_β, respectively.

https://dx.doi.org/10.1021/acs.jpca.0c02074
J. Phys. Chem. A 2020, 124, 2785–2791

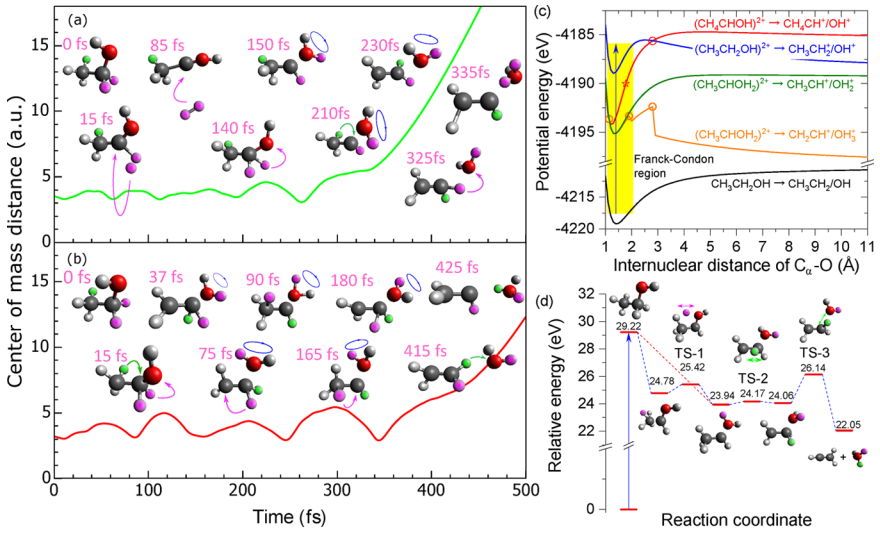

Figure 5. Pathways for H_3O^+ formation dynamics. (a) C_α as donor contributes two hydrogens to the final H_3O^+. (b) Both C_α and C_β are donors, and each contributes one hydrogen to the final H_3O^+. (c) Potential energy curves as a function of internuclear distance of C_α–O. (d) Reaction coordinate associates three transition states for H_3O^+ production. The open circles and star in panel (c) mark the possible transition states. The arrows in panel (d) indicate the main feature of vibration mode. The pink and green hydrogens belong to C_α and C_β in the neutral ethanol, respectively.

Figure 5 shows the H_3O^+ emission dynamics according to channel 3, which requires double hydrogen migration.[37] It also involves the stabilization mechanisms mentioned above. From the AIMD simulation, we can identify two reaction pathways. The first case shown in Figure 5a starts with H_2 roaming, while the second one in Figure 5b starts with hydrogen transfer from C_β to C_α. Both reactions lead to the intermediate product $CH_3CHOH_2^{2+}$, which is formed after around 150 fs for the H_2 roaming channel (Figure 5a) and after 90 fs for the hydrogen transfer channel (Figure 5b). Then both channels show a similar roaming of H_2O in the vicinity of C_α during which one hydrogen transfers from C_β to C_α. This transfer evolves on a rather flat PES (see Figure 5d) and results in long-time roaming of H_2O before it finally captures one proton from C_α.

The analysis of the static PES shows two possible ways to form the intermediate $CH_3CHOH_2^{2+}$: (i) hydrogen transfers from C_α to the hydroxyl group (see the red dashed line in Figure 5d),

$$CH_3CH_2OH^{2+} \rightarrow CH_3CHOH_2^{2+} \quad (4)$$

and (ii) hydrogen transfers from C_α to C_β in the first step and then transfers from C_β to the hydroxyl group

$$CH_3CH_2OH^{2+} \rightarrow CH_4CHOH^{2+} \rightarrow CH_3CHOH_2^{2+} \quad (5)$$

In Figure 5c, the PESs of different isomers are shown as a function of the C_α–O bond length, which eventually breaks for H_3O^+ emission. Without hydrogen transfer, the ethanol dication does not dissociate through C_α–O bond breakage. As shown by the blue curve in Figure 5c, the PES of $CH_3CH_2OH^+$ as a function of the C_α–O bond length shows a high potential barrier, which closes the dissociation channel. The isomeric transformation from $CH_3CH_2OH^{2+}$ to CH_4CHOH^{2+} associated with a C_α–O length increase only is also energetically forbidden due to the high potential energy barrier as marked by the red circle in Figure 5c. One possible pathway is expected, similar to that involved in C_α–C_β dissociation as shown in Figure 2f where a bond length increase is accompanied by hydrogen transfer. The energy level of such TS is marked by a red star in Figure 5c, which can be reached in the Franck–Condon region. Then the isomeric transformation from CH_4CHOH^{2+} to $CH_3CHOH_2^{2+}$ occurs at their PES crossing point as shown by the left orange circle in Figure 5c. The relaxed PES scanning of the stable dication, i.e., $CH_3CHOH_2^{2+}$, is shown by the orange curve in Figure 5c. With increasing C_α–O bond length, one hydrogen from C_β first transfers to C_α forming $CH_2CH_2OH_2^{2+}$ and then transfers to oxygen emitting finally H_3O^+, as shown by the middle and right orange circles in Figure 5c. The associated TSs and their pathways are confirmed by the IRC calculations as shown in Figure 5d. The flat PES around TS-1 and TS-2 means that the double hydrogen migration has a relatively long lifetime before dissociation.

CONCLUSIONS

To summarize, the present study demonstrates for ethanol that the ultrafast PT can give rise to a competition between CE on the repulsive PES and isomerization and thereby influence the fragmentation pathway. Our molecular dynamics simulations and PES calculations show that hydrogen migration can stabilize the repulsive state of the ethanol dication before CE opening up new pathways. For the ethanol dication, there are three possible ways to stabilize the dication, i.e., hydrogen transfer from C_α to C_β, from carbon to hydroxyl, and the formation of intermediate H_2. All of the stabilization processes can take place within 25 fs, which is faster than CE.

It is worthwhile to note that the roaming trajectories can be far away from the IRC paths of the TSs, which can be seen by comparing the simulated trajectories and the IRC paths. This is the case in particular for the TSa-3 in Figure 4g where a very high potential barrier is observed. The wide range roaming of H_2, as shown in Figure 4d,e, makes it possible to bypass the saddle point.[33] The roaming chemistry also challenges the conventional TS theory in predicting KER of associated channels. As obtained in Figures 4f,g and 5d, the energy difference between the highest energy level and the dissociation limit, which determines the KER, is always larger

https://dx.doi.org/10.1021/acs.jpca.0c02074
J. Phys. Chem. A 2020, 124, 2785–2791

than the averaged KER of the experiment and AIMO results, which are shown in Figure 1d,e. This is due to the fact that the roaming process will lead to highly excited vibrational levels of final H_3^+ and H_3O^+. As a result, the KER of the experiment and AIMD is lower than that predicted by a static energy calculation.

■ ASSOCIATED CONTENT

Supporting Information

The Supporting Information is available free of charge at https://pubs.acs.org/doi/10.1021/acs.jpca.0c02074.

Additional information on experimental methods and computational methods (PDF)

■ AUTHOR INFORMATION

Corresponding Authors

Xueguang Ren − *Max Planck Institut für Kernphysik, 69117 Heidelberg, Germany; School of Science, Xi'an Jiaotong University, Xi'an 710049, China*; Email: ren@mpi-hd.mpg.de

Alexander Dorn − *Max Planck Institut für Kernphysik, 69117 Heidelberg, Germany*; orcid.org/0000-0002-8024-224X; Email: dornalex@mpi-hd.mpg.de

Authors

Enliang Wang − *Max Planck Institut für Kernphysik, 69117 Heidelberg, Germany*; orcid.org/0000-0002-5703-6501

Xu Shan − *Hefei National Laboratory for Physical Sciences at Microscale and Department of Modern Physics, University of Science and Technology of China, Hefei, Anhui 230026, China*

Lei Chen − *Hefei National Laboratory for Physical Sciences at Microscale and Department of Modern Physics, University of Science and Technology of China, Hefei, Anhui 230026, China*

Thomas Pfeifer − *Max Planck Institut für Kernphysik, 69117 Heidelberg, Germany*

Xiangjun Chen − *Hefei National Laboratory for Physical Sciences at Microscale and Department of Modern Physics, University of Science and Technology of China, Hefei, Anhui 230026, China*; orcid.org/0000-0002-4354-9330

Complete contact information is available at: https://pubs.acs.org/10.1021/acs.jpca.0c02074

Notes

The authors declare no competing financial interest.

■ ACKNOWLEDGMENTS

This work is jointly supported by the National Natural Science Foundation of China (Grant Nos. 11534011, 11774281, and 11327404) and the National Key Research and Development Program of China (Grant No. 2017YFA0402300). X.R. is grateful for support from DFG project No. RE 2966/3-1. E.W. acknowledges a fellowship from the Alexander von Humboldt Foundation.

■ REFERENCES

(1) Thissen, R.; Witasse, O.; Dutuit, O.; Wedlund, C. S.; Gronoff, G.; Lilensten, J. Doubly-charged ions in the planetary ionospheres: a review. *Phys. Chem. Chem. Phys.* **2011**, *13*, 18264−18287.

(2) Böhme, D. K. Multiply-charged ions and interstellar chemistry. *Phys. Chem. Chem. Phys.* **2011**, *13*, 18253−18263.

(3) Price, S. D.; Roithová, J. Multiply charged ions in the gas phase. *Phys. Chem. Chem. Phys.* **2011**, *13*, 18251−18252.

(4) Schröder, D. Coulomb Explosions and Stability of Multiply Charged Ions in the Gas Phase. *Angew. Chem. Int. Ed.* **2004**, *43*, 1329−1331.

(5) Tuckerman, M. E.; Marx, D.; Klein, M. L.; Parrinello, M. On the Quantum Nature of the Shared Proton in Hydrogen Bonds. *Science* **1997**, *275*, 817−820.

(6) Xu, S.; Guo, D.; Ma, X.; Zhu, X.; Feng, W.; Yan, S.; Zhao, D.; Gao, Y.; Zhang, S.; Ren, X.; Zhao, Y.; Xu, Z.; Dorn, A.; Cederbaum, L. S.; Kryzhevoi, N. V. Damaging Intermolecular Energy and Proton Transfer Processes in Alpha-Particle-Irradiated Hydrogen-Bonded Systems. *Angew. Chem. Int. Ed.* **2018**, *57*, 17023−17027.

(7) Sun, Z.; Siu, C.-K.; Balaj, O. P.; Gruber, M.; Bondybey, V. E.; Beyer, M. K. Proton Transfer in Ionic Water Clusters. *Angew. Chem. Int. Ed.* **2006**, *45*, 4027−4030.

(8) Hynes, J.; Klinman, J.; Limbach, H.; Schowen, R. *Hydrogen-Transfer Reactions*. Wiley-VCH: 2007.

(9) Douhal, A.; Kim, S. K.; Zewail, A. H. Femtosecond molecular dynamics of tautomerization in model base pairs. *Nature* **1995**, *378*, 260−263.

(10) Kwon, O.-H.; Zewail, A. H. Double proton transfer dynamics of model DNA base pairs in the condensed phase. *Proc. Natl. Acad. Sci. U. S. A.* **2007**, *104*, 8703−8708.

(11) Löwdin, P.-O. Proton Tunneling in DNA and its Biological Implications. *Rev. Mod. Phys.* **1963**, *35*, 724−732.

(12) Zhang, Y.; de La Harpe, K.; Beckstead, A. A.; Improta, R.; Kohler, B. UV-Induced Proton Transfer between DNA Strands. *J. Am. Chem. Soc.* **2015**, *137*, 7059−7062.

(13) Röttger, K.; Marroux, H. J. B.; Grubb, M. P.; Coulter, P. M.; Böhnke, H.; Henderson, A. S.; Galan, M. C.; Temps, F.; Orr-Ewing, A. J.; Roberts, G. M. Ultraviolet Absorption Induces Hydrogen-Atom Transfer in G·C Watson−Crick DNA Base Pairs in Solution. *Angew. Chem. Int. Ed.* **2015**, *127*, 14932−14935.

(14) Pérez de Tudela, R.; Marx, D. Water-Induced Zwitterionization of Glycine: Stabilization Mechanism and Spectral Signatures. *J. Phys. Chem. Lett.* **2016**, *7*, 5137−5142.

(15) Maclot, S.; Piekarski, D. G.; Domaracka, A.; Méry, A.; Vizcaino, V.; Adoui, L.; Martín, F.; Alcamí, M.; Huber, B. A.; Rousseau, P.; Díaz-Tendero, S. Dynamics of Glycine Dications in the Gas Phase: Ultrafast Intramolecular Hydrogen Migration versus Coulomb Repulsion. *J. Phys. Chem. Lett.* **2013**, *4*, 3903−3909.

(16) Castrovilli, M. C.; Trabattoni, A.; Bolognesi, P.; O'Keeffe, P.; Avaldi, L.; Nisoli, M.; Calegari, F.; Cireasa, R. Ultrafast Hydrogen Migration in Photoionized Glycine. *J. Phys. Chem. Lett.* **2018**, *9*, 6012−6016.

(17) Tuckerman, M. E.; Marx, D.; Parrinello, M. The nature and transport mechanism of hydrated hydroxide ions in aqueous solution. *Nature* **2002**, *417*, 925−929.

(18) Li, X.-Z.; Walker, B.; Michaelides, A. Quantum nature of the hydrogen bond. *Proc. Natl. Acad. Sci. U. S. A.* **2011**, *108*, 6369−6373.

(19) Ceriotti, M.; Fang, W.; Kusalik, P. G.; McKenzie, R. H.; Michaelides, A.; Morales, M. A.; Markland, T. E. Nuclear Quantum Effects in Water and Aqueous Systems: Experiment, Theory, and Current Challenges. *Chem. Rev.* **2016**, *116*, 7529−7550.

(20) Koch, M.; Pagan, M.; Persson, M.; Gawinkowski, S.; Waluk, J.; Kumagai, T. Direct Observation of Double Hydrogen Transfer via Quantum Tunneling in a Single Porphycene Molecule on a Ag(110) Surface. *J. Am. Chem. Soc.* **2017**, *139*, 12681−12687.

(21) Richter, C.; Hollas, D.; Saak, C.-M.; Förstel, M.; Miteva, T.; Mucke, M.; Björneholm, O.; Sisourat, N.; Slavíček, P.; Hergenhahn, U. Competition between proton transfer and intermolecular Coulombic decay in water. *Nat. Commun.* **2018**, *9*, 4988.

(22) Kamarchik, E.; Koziol, L.; Reisler, H.; Bowman, J. M.; Krylov, A. I. Roaming Pathway Leading to Unexpected Water + Vinyl Products in C2H4OH Dissociation. *J. Phys. Chem. Lett.* **2010**, *1*, 3058−3065.

(23) Piekarski, D. G.; Delaunay, R.; Maclot, S.; Adoui, L.; Martín, F.; Alcamí, M.; Huber, B. A.; Rousseau, P.; Domaracka, A.; Díaz-Tendero, S. Unusual hydroxyl migration in the fragmentation of *β*-

alanine dication in the gas phase. *Phys. Chem. Chem. Phys.* **2015**, *17*, 16767−16778.
(24) Jiang, Y. H.; Rudenko, A.; Herrwerth, O.; Foucar, L.; Kurka, M.; Kühnel, K. U.; Lezius, M.; Kling, M. F.; van Tilborg, J.; Belkacem, A.; Ueda, K.; Düsterer, S.; Treusch, R.; Schröter, C. D.; Moshammer, R.; Ullrich, J. Ultrafast Extreme Ultraviolet Induced Isomerization of Acetylene Cations. *Phys. Rev. Lett.* **2010**, *105*, 263002.
(25) Li, Z.; Inhester, L.; Liekhus-Schmaltz, C.; Curchod, B. F. E.; Snyder, J. W. J.; Medvedev, N.; Cryan, J.; Osipov, T.; Pabst, S.; Vendrell, O.; Bucksbaum, P.; Martinez, T. J. Ultrafast isomerization in acetylene dication after carbon K-shell ionization. *Nat. Commun.* **2017**, *8*, 453−453.
(26) Xu, S.; Zhao, H.; Zhu, X.; Guo, D.; Feng, W.; Lau, K.-C.; Ma, X. Dissociation of $[HCCH]_2^+$ to H_2^+ and C_2^+: a benchmark reaction involving H migration, H−H combination, and C−H bond cleavage. *Phys. Chem. Chem. Phys.* **2018**, *20*, 27725−27729.
(27) Dermota, T. E.; Zhong, Q.; Castleman, A. W. Ultrafast Dynamics in Cluster Systems. *Chem. Rev.* **2004**, *104*, 1861−1886.
(28) De, S.; Rajput, J.; Roy, A.; Ghosh, P. N.; Safvan, C. P. Formation of H_3^+ due to Intramolecular Bond Rearrangement in Doubly Charged Methanol. *Phys. Rev. Lett.* **2006**, *97*, 213201.
(29) Schirmel, N.; Reusch, N.; Horsch, P.; Weitzel, K.-M. Formation of fragment ions (H^+, H_3^+, CH_3^+) from ethane in intense femtosecond laser fields − from understanding to control. *Faraday Discuss.* **2013**, *163*, 461−474.
(30) Ekanayake, N.; Nairat, M.; Kaderiya, B.; Feizollah, P.; Jochim, B.; Severt, T.; Berry, B.; Pandiri, K. R.; Carnes, K. D.; Pathak, S.; Rolles, D.; Rudenko, A.; Ben-Itzhak, I.; Mancuso, C. A.; Fales, B. S.; Jackson, J. E.; Levine, B. G.; Dantus, M. Mechanisms and time-resolved dynamics for trihydrogen cation (H_3^+) formation from organic molecules in strong laser fields. *Sci. Rep.* **2017**, *7*, 4703.
(31) Ando, T.; Shimamoto, A.; Miura, S.; Iwasaki, A.; Nakai, K.; Yamanouchi, K. Coherent vibrations in methanol cation probed by periodic H_3^+ ejection after double ionization. *Commun. Chem.* **2018**, *1*, 7.
(32) Ekanayake, N.; Severt, T.; Nairat, M.; Weingartz, N. P.; Farris, B. M.; Kaderiya, B.; Feizollah, P.; Jochim, B.; Ziaee, F.; Borne, K.; Raju, P. K.; Carnes, K. D.; Rolles, D.; Rudenko, A.; Levine, B. G.; Jackson, J. E.; Ben-Itzhak, I.; Dantus, M. H_2 roaming chemistry and the formation of H_3^+ from organic molecules in strong laser fields. *Nat. Commun.* **2018**, *9*, 5186.
(33) Townsend, D.; Lahankar, S. A.; Lee, S. K.; Chambreau, S. D.; Suits, A. G.; Zhang, X.; Rheinecker, J.; Harding, L.; Bowman, J. M. The roaming atom: straying from the reaction path in formaldehyde decomposition. *Science* **2004**, *306*, 1158−1161.
(34) Ekanayake, N.; Nairat, M.; Weingartz, N. P.; Michie, M. J.; Levine, B. G.; Dantus, M. Substituent effects on H_3^+ formation via H_2 roaming mechanisms from organic molecules under strong-field photodissociation. *J. Chem. Phys.* **2018**, *149*, 244310.
(35) Itakura, R. T. T.; Hishikawa, A.; Yamanouchi, K. Coincidence momentum imaging of two- and three-body Coulomb explosion of ethanol in intense laser fields. In *Ultrafast Optics V*; *Springer Series in Optical Sciences 132*; Watanabe, S., Ed.; Springer: 2007; pp 375−376.
(36) Linusson, P.; Stenrup, M.; Larson, Å.; Andersson, E.; Heijkenskjöld, F.; Andersson, P.; Eland, J. H. D.; Karlsson, L.; Rubensson, J. E.; Feifel, R. Double photoionization of alcohol molecules. *Phys. Rev. A* **2009**, *80*, No. 032516.
(37) Kling, N. G.; Díaz-Tendero, S.; Obaid, R.; Disla, M. R.; Xiong, H.; Sundberg, M.; Khosravi, S. D.; Davino, M.; Drach, P.; Carroll, A. M.; Osipov, T.; Martín, F.; Berrah, N. Time-resolved molecular dynamics of single and double hydrogen migration in ethanol. *Nat. Commun.* **2019**, *10*, 2813.

https://dx.doi.org/10.1021/acs.jpca.0c02074
J. Phys. Chem. A 2020, 124, 2785−2791